Collective rotational bands at low excitation energy in ^{186}Os: Vibrational and rotational degrees of freedom

L. Mdletshe,[1,2,*] X. Q. Yang,[3] E. A. Lawrie,[2,4] M. A. Sithole,[1,2,4] S. N. T. Majola,[5,1,2] S. S. Ntshangase,[1]
J. F. Sharpey-Schafer,[1] J. J. Lawrie,[2,4] S. H. Mthembu,[4,2] T. D. Bucher,[4,2] L. Msebi,[4,2] R. A. Bark,[2] A. A. Avaa,[2,6,†]
M. V. Chisapi,[2,7] P. Jones,[2] S. Jongile,[2,7] Z. P. Li,[3] L. Makhathini,[2,7] K. L. Malatji,[2,7] A. A. Netshiya,[8,2,6] Z. Shi,[9] B. Y. Song,[3]
L. Wang,[3] J. Xiang,[3] and S. Q. Zhang[10]

[1]*Department of Physics, University of Zululand, P/B X1001, KwaDlangezwa 3886, South Africa*
[2]*iThemba LABS, National Research Foundation, P.O. Box 722, Somerset West 7129, South Africa*
[3]*School of Physical Science and Technology, Southwest University, Chongqing 400715 China*
[4]*Department of Physics, University of the Western Cape, P/B X17, Bellville 7535, South Africa*
[5]*Department of Physics, University of Johannesburg, P.O. Box 524, Auckland Park 2006, South Africa*
[6]*School of Physics, University of the Witwatersrand, Johannesburg 2000, South Africa*
[7]*Department of Physics, University of Stellenbosch, P/B X1, Matieland 7602, South Africa*
[8]*Walter Sisulu University, P/B X1, Unitra 5117, South Africa*
[9]*School of Physics and Nuclear Energy Engineering, Beihang University, Beijing 100191, China*
[10]*State Key Laboratory of Nuclear Physics and Technology, School of Physics, Peking University, Beijing 100871, China*

Collective structures in ^{186}Os have been investigated through the ^{186}W(^{4}He, $4n$) ^{186}Os reaction, at a beam energy of 48 MeV. The low-lying bands built on the excited 0_2^+, 2_2^+, and 4_3^+ states have been extended up to spins of 12^+, 15^+, and 8^+, respectively, and a number of new linking transitions were identified. The features of the collective bands in ^{186}Os, such as level energies, are presented in the context of a systematic study of the neighboring even-even $^{182–192}$Os isotopes. In addition, the validity of the K-selection rule, stemming from a description based on axial symmetry of the nuclear shape, is examined. The observed decays between the rotational bands support a description where K is conserved. However, some K-forbidden decays were also identified, suggesting that a model allowing for small K admixtures is probably required. The experimental data are further compared with calculations using a five-dimensional collective Hamiltonian based on covariant density functional theory. The calculations predict that the collective bands are associated with different nuclear shapes, varying in quadrupole deformation, triaxiality, and softness.

I. INTRODUCTION

In nuclear structure physics one of the central challenges is to properly understand the nature of the structures built on the excited 0_2^+, 2_2^+, and 4_3^+ states in even-even (e-e) deformed nuclei. Traditionally, these structures have been interpreted as due to vibrations of the nuclear shape [1]. These were modeled by excitations in a potential $V(\beta, \gamma)$ depending on the quadrupole deformation (β) and triaxiality (γ), initially assuming that the β and γ degrees of freedom could be separated adiabatically, $V(\beta, \gamma) = V(\beta) + V(\gamma)$, and that both $V(\beta)$ and $V(\gamma)$ could be represented by simple harmonic oscillator (SHO) potentials [1]. In this model the structures are due to SHO quadrupole phonon excitations in the $V(\beta, \gamma)$ potential. For instance the band built above the 0_2^+ level corresponds to a one-phonon vibration with respect to the quadrupole deformation β, thus these bands were called β bands. Here the phonon carries zero angular momentum. The 2_2^+ γ band corresponds to a one-phonon γ vibration where the phonon carries $2\hbar$ of angular momentum that is aligned along the symmetry axis. Thus the projection of the total angular momentum along the symmetry axis is conserved and $K = 2$. Within this model the 4_3^+ γ band corresponds to the excitation of two γ phonons where the projection on the symmetry axis is $K = 4$; for a detailed description see Ref. [2].

It was first pointed out by Davydov and Philippov [3] that there was an alternative interpretation for the 2_2^+ and 4_3^+ γ bands, where these bands resulted from the rotation of a deformed nuclear shape that is axially asymmetric (see also [1,2], and [4,5]). Such nuclei could rotate around all their three axes [three-dimensional (3D) rotation], which looks like precession of the total angular momentum around the intermediate nuclear axis in a similar way as a rotating top precesses around the vertical direction. For these bands the projection of the total angular momentum along any of the nuclear axes is only approximately conserved at low spins.

Experimental data collected over recent decades have also led to suggestions that the experimentally observed 0_2^+ bands in many deformed nuclei may have nonvibrational nature [6–8]. The natures of the 0_2^+, 2_2^+, and 4_3^+ bands have been studied intensively, particularly at the beginning of the neutron $N = 82$–126 shell [6–19]; however, there are still many open questions.

The ^{186}Os nucleus lies towards the upper end of the $N = 82$–126 shell. For the Os isotopic chain the nuclear quadrupole deformation decreases when the neutron number increases. The deformed e-e $^{182-192}$Os nuclei have 2^+ γ bands at low excitation energies, in particular the 2_2^+ band in ^{192}Os has the lowest excitation energy among all known γ bands in the nuclear chart. Furthermore the excitation energy of the 2_2^+ band decreases for the heavier isotopes, which suggests that the triaxiality degree of freedom plays a more significant role for them. This makes the Os isotopes one of the best regions to study the influence of the γ degree of freedom on the observed rotational bands.

The bandheads of the 4_3^+ γ bands in the e-e Os isotopes have excitation energies that are approximately twice the excitation energies of the bandheads of the 2^+ γ bands, making them excellent candidates for two γ phonon excitations. Such a vibrational interpretation was proposed and also supported by measurements of the nuclear shape parameters in a Coulomb excitation experiment [20]. However, the 4_3^+ bandheads are also strongly populated in stripping and pickup reactions as well as in inelastic scattering; see Refs. [14,21,22]. Such a strong population is incompatible with a two-phonon vibrational nature, but suggests that the 4^+ bands have dominant two-proton single-particle configuration. A large hexadecapole component was also inferred in these measurements supporting a $K = 4$ nature of this band. Bands based on particle-hole excitations can have strong $M1$ transitions between even- and odd-spin members of the band while a hexadecapole shape will allow direct $E4$ transitions between the 4^+ bandhead and the ground state.

Almond *et al.* [23] have reanalyzed the Coulomb-excitation data for the e-e $^{186-192}$Os of Wu *et al.* [20] using a triaxial-rotor model with independent inertia and electric quadrupole tensors. They find that triaxiality improves the agreement with the experimental data for the 2_2^+ bands, but not for the 4^+ bands. In a phonon model $E_{4_3^+}/E_{2_2^+} = 2$, whereas in a rigid triaxial model this ratio depends on the γ deformation, it is approximately 4 for $\gamma = 30°$.

It should be noted that the available information on the 4_3^+ bands in these Os nuclei is scarce, particularly for the lighter isotopes where experimental data is limited to the first two states only. This does not allow the study of the moments of inertia of these bands and whether there are strong $M1$ transitions linking the even- and odd-spin states. To give more insight into the underlying microscopic identity of the low-lying bands in the Os isotopes, we performed an experiment on ^{186}Os, and compared the results with those of the neighboring Os isotopes. The features of the linking transitions between the low-energy bands were also reexamined. The 4_3^+ band was confirmed and extended up to higher spins. The findings from this work are discussed in terms of a simple vibrational-phonon model and a triaxial-rotor model. In addition, new results from a model based on the five-dimensional collective Hamiltonian coupled with the covariant density functional theory (5DCH-CDFT) [24,25] for the 4_3^+ band are presented and compared with experimental data. Similar calculations have been used to reproduce the experimental observations for the low-lying 0_2^+ and 2_2^+ bands in the $A \approx 160$ mass region [9] and for a systematic study of the nuclei in the Er to Pt region [26].

II. EXPERIMENTAL DETAILS AND DATA ANALYSIS

The excited states in ^{186}Os were populated using the ^{186}W(^{4}He, $4n$) ^{186}Os reaction, at a beam energy of 48 MeV. A beam of ^{4}He ions was provided by the iThemba LABS Separated-Sector Cyclotron (SSC), and was used to bombard a stack of four ^{186}W targets with a thickness of 100 μg/cm^2 each, making a total thickness of 400 μg/cm^2. The stacked targets were placed at the center of the target chamber, surrounded by the high purity germanium (HPGe) clover detectors of the AFRODITE γ-ray spectrometer [27]. A total of 11 clover detectors were used to detect the γ rays that were emitted during the experiment, 7 positioned at an angle of 90° and 4 at 135° with respect to the beam direction. A total of about 5×10^9 γ-γ coincidence events were recorded during the experiment.

The data were sorted into E_γ-E_γ matrices through which the level scheme of ^{186}Os was built. The spins and parities of the previously known and new levels were measured using angular distribution ratios (R_{AD}) and linear polarization asymmetry A_p. The coincidence data were sorted into two asymmetric matrices, where one axis corresponded to γ-ray energies deposited in the clover detectors positioned at 135° and 90°, respectively, while the γ-ray energies deposited in all detectors were placed on the second axis. We measured R_{AD} ratios using

$$R_{AD} = \frac{I_{\gamma_1}^{135°}\left(\text{Gated}_{\gamma_2}^{\text{all}}\right)}{I_{\gamma_1}^{90°}\left(\text{Gated}_{\gamma_2}^{\text{all}}\right)}, \tag{1}$$

where $I_{\gamma_1}^{135°}(\text{Gated}_{\gamma_2}^{\text{all}})$ represents the coincidence intensity of γ_1 detected at 135°, gated with γ_2 registered in all detectors. Similarly, $I_{\gamma_1}^{90°}(\text{Gated}_{\gamma_2}^{\text{all}})$, denotes the coincidence intensity of γ_1 detected at 90°, gated with γ_2 in all detectors. When a gate is made on a quadrupole transition, values of R_{AD} of ≈ 0.8 and ≈ 1.2 were found for pure stretched dipole and quadrupole transitions, respectively.

Linear polarization measurements were performed to distinguish the possible electric or magnetic nature of the γ-ray transitions. A polarization matrix was constructed from the data corresponding to the energy detected in any detector on one axis, while the other axis corresponds to the energy of a Compton scattered γ ray in a perpendicular or parallel direction inside a clover detector with respect to the beam direction. The polarization asymmetries (A_P) were calculated using

$$A_P = \frac{aN_V - N_H}{aN_V + N_H}, \tag{2}$$
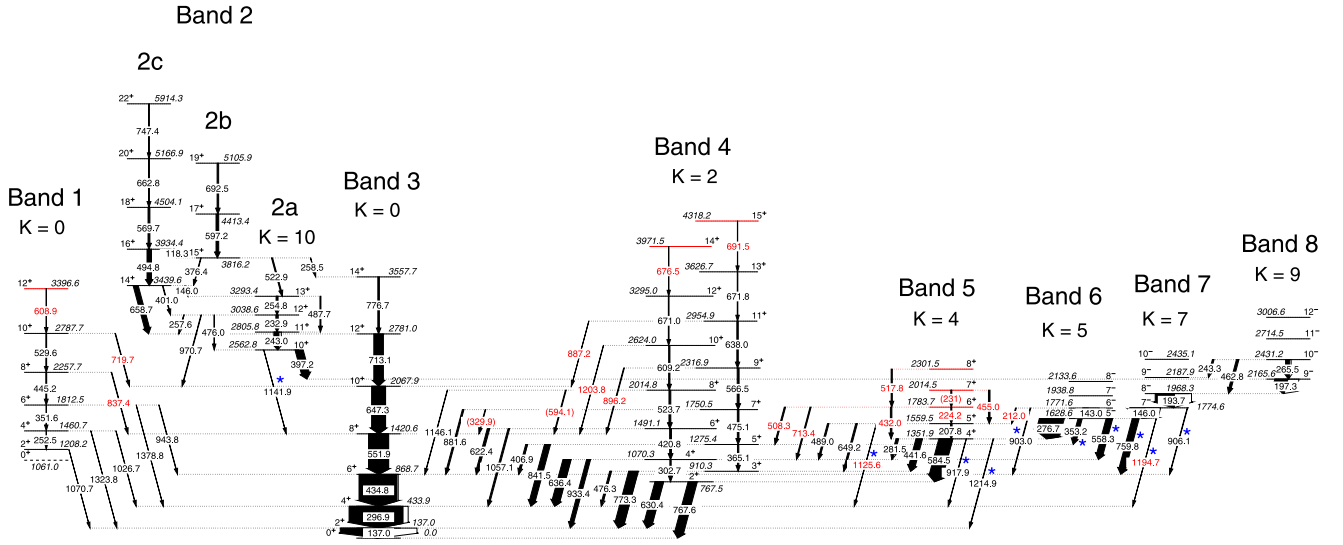
FIG. 1. Partial decay scheme of ^{186}Os established in the present work. The previously known levels and transitions are labeled in black while the new ones are shown in red. The transitions marked with blue asterisks are forbidden by the K-selection rule. The widths of the arrows are proportional to the transition intensities, and the energies are given in keV.

where N_V and N_H are the number of γ rays scattered between the crystals of a clover detector at 90° perpendicular and parallel to the beam direction respectively, and a is the relative efficiency parameter, given by N_H/N_V for the γ rays of the ^{152}Eu source. For pure stretched transitions, positive and negative A_P values indicate electric and magnetic nature, respectively.

III. EXPERIMENTAL RESULTS

Figure 1 shows the partial decay scheme of ^{186}Os obtained in the present study where 20 new transitions were added with respect to previous works [28,29]. Most of the new transitions are part of the 0_2^+, 2_2^+, and 4_3^+ positive-parity structures. The previously reported negative-parity bands (Bands 6, 7, and 8) of ^{186}Os were also observed in our data. They are not shown in Fig. 1, except for the levels near their bandheads, which are relevant to the discussion.

The bandheads of Bands 7 and 8 are isomeric states with half-lives of 8.36(24) and 5.7(4) ns, respectively [30]. In our experiment we used thin-foil targets, thus the residual nuclei recoiled out of the target. While prompt transitions are emitted at the center of the array, transitions that are positioned below an isomeric state are emitted when the nuclei have recoiled out of the target. The detector efficiency for such delayed transitions is affected by the shadowing of their collimators. We observed a mismatch between the measured feeding and depopulating intensities for the two isomeric levels and also for some levels that are strongly populated by the isomeric decays, such as the 5^- level at 1629 keV and the 4^+ level at 1352 keV. To avoid possible impact on the measured R_{AD} ratios and A_P asymmetry for transitions at low spins, gates that bypass the isomeric feeding were selected. Experimental details about the observed γ rays are listed in Table I and described below.

The excited states of the 0_2^+ band, Band 1, decay strongly toward the ground-state band, particularly at low spins, resulting in low intraband intensity near the bandhead. As in previous works we could not observe the $2^+ \rightarrow 0^+$ intraband transition, thus the previously identified 0_2^+ level at 1061 keV is only tentatively associated with Band 1. This band was extended to higher spins by adding one new level and three new transitions, as shown in Fig. 1. The new transitions are illustrated in Fig. 2, where two spectra gated on the 530- and 609-keV transitions are displayed. The measured R_{AD} ratios for the intraband transitions are consistent with stretched quadrupole nature. The R_{AD} ratios for the transitions linking this band to the ground-state band support the current spin assignments of Band 1, as they suggest stretched quadrupole ($\Delta I = 2$) or unstretched dipole ($\Delta I = 0$) nature.

The previously observed states of the 2_2^+ γ band, Band 4, were confirmed and the band was extended by two new levels and seven new transitions, as shown in Fig. 1. The new transitions are illustrated in the gated spectra of Fig. 3. Band 4 consists of two sequences of $E2$ transitions linking its even- and odd-spin members, respectively. The three previously reported intraband transitions linking these two sequences of 143 keV ($3^+ \rightarrow 2^+$), 161 keV ($4^+ \rightarrow 3^+$), and 216 keV ($6^+ \rightarrow 5^+$), could not be identified in our data. Their reported γ-ray branching intensities are 3.3, 1.0, and 3.2, respectively [30]. Our data suggest that if these transitions exist, their branchings are less than 1%. The measured R_{AD} ratios for the intraband $E2$ transitions are consistent with stretched quadrupole nature. The measured R_{AD} ratios for the interband $\Delta I = 0$, 1, and 2 transitions are consistent with the present spin assignments. The previously observed $\Delta I = 1$ transitions decaying from the γ band to the ground-state band were assigned almost pure (more than 99%) unstretched $E2$ nature [30]. The values, measured in this work, of R_{AD} of ≈ 0.8 for these transitions and for the newly observed

TABLE I. The γ-ray energies (E_γ) and the corresponding γ-ray intensities (I_γ), angular distribution ratios (R_{AD}), and linear polarization asymmetries (A_P) for the transition of ^{186}Os, shown in Fig. 1. The energies of the initial states (E_i) and the band where the transitions feed into (Band no.), as well as the spin assignment for the initial (I_i^π) and final (I_f^π) states are also listed. The measured γ-ray energies have uncertainties of 0.3 keV and up to 0.5 keV for the weaker and doublet transitions. Information that could not be obtained is indicated with a dash symbol.

E_i	E_γ	I_γ	$I_i^\pi \rightarrow I_f^\pi$	R_{AD}	A_P	Band no.
Band 1						
1208.2	1070.7	0.41(15)	$2^+ \rightarrow 2^+$	–	–	3
1460.7	252.5	0.08(4)	$4^+ \rightarrow 2^+$	–	–	1
1460.7	1026.7	0.5(2)	$4^+ \rightarrow 4^+$	1.4(3)	–	3
1460.7	1323.8	0.4(1)	$4^+ \rightarrow 2^+$	1.6(7)	–	3
1812.5	351.6	0.8(1)	$6^+ \rightarrow 4^+$	1.2(2)	–	1
1812.5	943.8	0.7(1)	$6^+ \rightarrow 6^+$	1.0(2)	–	3
1812.5	1378.8	0.3(1)	$6^+ \rightarrow 4^+$	1.1(3)	–	3
2257.7	445.2	1.6(2)	$8^+ \rightarrow 6^+$	1.3(2)	–	1
2257.7	837.4	0.3(1)	$8^+ \rightarrow 8^+$	–	–	3
2787.7	529.6	1.4(2)	$10^+ \rightarrow 8^+$	1.3(2)	–	1
2787.7	719.7	0.3(1)	$10^+ \rightarrow 10^+$	–	–	3
3396.6	608.9	0.8(2)	$12^+ \rightarrow 10^+$	1.4(2)	–	1
Band 2a						
2562.8	397.2	14.5(5)	$10^+ \rightarrow 9^-$	0.84(5)	0.05(2)	8
2562.8	1141.9	0.30(5)	$10^+ \rightarrow 8^+$	–		3
2805.8	243.0	9.4(3)	$11^+ \rightarrow 10^+$	0.58(6)		2a
3038.6	232.9	2.9(3)	$12^+ \rightarrow 11^+$	0.63(9)	–	2a
3038.6	257.6	0.6(1)	$12^+ \rightarrow 12^+$	–	–	3
3038.6	476.0	0.7(1)	$12^+ \rightarrow 10^+$	1.22(13)	–	2a
3038.6	970.7	1.0(1)	$12^+ \rightarrow 10^+$	–	–	3
3293.4	254.8	2.6(2)	$13^+ \rightarrow 12^+$	0.68(9)	–	2a
3293.4	487.7	1.7(2)	$13^+ \rightarrow 11^+$	1.31(9)	0.03(3)	2a
Band 2b						
3816.2	258.5	0.4(1)	$15^+ \rightarrow 14^+$	–	–	3
3816.2	376.4	0.9(1)	$15^+ \rightarrow 14^+$	–	–	2c
3816.2	522.9	2.0(2)	$15^+ \rightarrow 13^+$	1.32(9)	–	2a
4413.4	597.2	2.5(5)	$17^+ \rightarrow 15^+$	–	–	2b
5105.9	692.5	2.0(5)	$19^+ \rightarrow 17^+$	–	–	2b
Band 2c						
3439.6	146.0	0.05(4)	$14^+ \rightarrow 13^+$	–	–	2a
3439.6	401.0	1.1(2)	$14^+ \rightarrow 12^+$	–	–	2a
3439.6	658.7	9.1(8)	$14^+ \rightarrow 12^+$	1.21(6)	0.04(2)	3
3934.4	118.3	0.4(1)	$16^+ \rightarrow 15^+$	–	–	2b
3934.4	494.8	8.1(5)	$16^+ \rightarrow 14^+$	1.24(7)	0.07(3)	2c
4504.1	569.7	3.4(5)	$18^+ \rightarrow 16^+$	1.05(16)	–	2c
5166.9	662.8	1.7(4)	$20^+ \rightarrow 18^+$	1.25(14)	–	2c
5914.3	747.4	0.5(2)	$22^+ \rightarrow 20^+$	1.3(7)	–	2c
Band 3						
137.0	137.0	62(3)	$2^+ \rightarrow 0^+$	1.10(6)	–	3
433.9	296.9	100(3)	$4^+ \rightarrow 2^+$	1.17(4)	0.05(2)	3
868.7	434.8	70(3)	$6^+ \rightarrow 4^+$	1.17(5)	0.03(2)	3
1420.6	551.9	37(2)	$8^+ \rightarrow 6^+$	1.19(6)	0.07(3)	3
2067.9	647.3	26(1)	$10^+ \rightarrow 8^+$	1.22(6)	0.04(2)	3
2781.0	713.1	18(1)	$12^+ \rightarrow 10^+$	1.23(6)	0.04(2)	3
3557.7	776.7	2.9(2)	$14^+ \rightarrow 12^+$	1.16(8)	0.06(4)	3
Band 4						
767.5	630.4	15(1)	$2^+ \rightarrow 2^+$	1.5(6)	–	3
767.5	767.6	17(1)	$2^+ \rightarrow 0^+$	1.5(6)	–	3
910.3	476.3	1.9(2)	$3^+ \rightarrow 4^+$	–	–	3

TABLE I. (*Continued.*)

E_i	E_γ	I_γ	$I_i^\pi \rightarrow I_f^\pi$	R_{AD}	A_P	Band no.
910.3	773.3	17(1)	$3^+ \rightarrow 2^+$	0.73(15)	–	3
1070.3	302.7	2.2(4)	$4^+ \rightarrow 2^+$	–	–	4
1070.3	636.4	14.2(5)	$4^+ \rightarrow 4^+$	0.8(3)	–	3
1070.3	933.4	11.9(6)	$4^+ \rightarrow 2^+$	1.2(3)	–	3
1275.4	365 .1	2.4(2)	$5^+ \rightarrow 3^+$	–	–	4
1275.4	406.9	1.4(2)	$5^+ \rightarrow 6^+$	–	–	3
1275.4	841.5	10.6(4)	$5^+ \rightarrow 4^+$	1.0(2)	–	3
1491.1	420.8	4.3(2)	$6^+ \rightarrow 4^+$	1.2(2)	–	4
1491.1	622.4	4.3(3)	$6^+ \rightarrow 6^+$	0.8(3)	–	3
1491.1	1057.1	3.9(3)	$6^+ \rightarrow 4^+$	1.0(2)	–	3
1750.5	(329.9)	0.3(1)	$7^+ \rightarrow 8^+$	–	–	3
1750.5	475.1	2.7(2)	$7^+ \rightarrow 5^+$	–	–	4
1750.5	881.6	2.8(2)	$7^+ \rightarrow 6^+$	0.75(14)	−0.08(6)	3
2014.8	523.7	3.3(2)	$8^+ \rightarrow 6^+$	1.3(3)	0.05(3)	4
2014.8	(594.1)	–	$8^+ \rightarrow 8^+$	–	–	3
2014.8	1146.1	0.4(1)	$8^+ \rightarrow 6^+$	1.3(5)	–	3
2316.9	566.5	3.5(2)	$9^+ \rightarrow 7^+$	1.3(3)	–	4
2316.9	896.2	1.3(2)	$9^+ \rightarrow 8^+$	0.84(14)	−0.14(8)	3
2624.0	609.2	2.4(2)	$10^+ \rightarrow 8^+$	1.3(2)	–	4
2624.0	1203.8	0.24(7)	$10^+ \rightarrow 8^+$	1.4(6)	–	3
2954.9	638.0	2.6(2)	$11^+ \rightarrow 9^+$	–	–	4
2954.9	887.2	0.41(6)	$11^+ \rightarrow 10^+$	0.8(2)	–	3
3295.0	671.0	1.24(9)	$12^+ \rightarrow 10^+$	–	–	4
3626.7	671.8	0.98(8)	$13^+ \rightarrow 11^+$	–	–	4
3971.5	676.5	0.51(5)	$14^+ \rightarrow 12^+$	1.2(2)	–	4
4318.2	691.5	0.50(5)	$15^+ \rightarrow 13^+$	1.3(3)	–	4
Band 5						
1351.9	281.5	3.5(8)	$4^+ \rightarrow 4^+$	–	–	4
1351.9	441.6	10.8(4)	$4^+ \rightarrow 3^+$	0.9(2)	–	4
1351.9	584.5	24.8(8)	$4^+ \rightarrow 2^+$	1.1(1)	–	4
1351.9	917.9	0.5(1)	$4^+ \rightarrow 4^+$	–	–	3
1351.9	1214.9	0.8(1)	$4^+ \rightarrow 2^+$	–	–	3
1559.5	207.8	1.7(2)	$5^+ \rightarrow 4^+$	1.3(2)	–	5
1559.5	489.0	2.5(2)	$5^+ \rightarrow 4^+$	–	–	4
1559.5	649.2	2.9(2)	$5^+ \rightarrow 3^+$	–	–	4
1559.5	1125.6	0.4(1)	$5^+ \rightarrow 4^+$	–	–	3
1783.7	224.2	0.9(2)	$6^+ \rightarrow 5^+$	–	–	5
1783.7	432.0	2.7(2)	$6^+ \rightarrow 4^+$	1.1(2)	–	5
1783.7	508.3	0.6(3)	$6^+ \rightarrow 5^+$	–	–	4
1783.7	713.4	0.7(4)	$6^+ \rightarrow 4^+$	–	–	4
2014.5	(231)	1.3(6)	$7^+ \rightarrow 6^+$	–	–	5
2014.5	455.0	2.8(2)	$7^+ \rightarrow 5^+$	1.3(4)	–	5
2301.5	517.8	2.1(2)	$8^+ \rightarrow 6^+$	1.1(4)	–	5
Band 6						
1628.6	276.7	43.5(13)	$5^- \rightarrow 4^+$	0.88(8)	–	5
1628.6	353.2	7.4(3)	$5^- \rightarrow 5^+$	1.08(9)	–	4
1628.6	558.3	11.7(4)	$5^- \rightarrow 4^+$	–	–	4
1628.6	759.8	12.3(4)	$5^- \rightarrow 6^+$	0.9(1)	–	3
1628.6	1194.7	0.16(7)	$5^- \rightarrow 4^+$	–	–	3
1771.6	143.0	9.7(3)	$6^- \rightarrow 5^-$	0.7(1)	–	6
1771.6	212.0	0.9(2)	$6^- \rightarrow 5^+$	–	–	5
1771.6	903.0	1.3(2)	$6^- \rightarrow 6^+$	–	–	3
Band 7						
1774.6	146.0	27.4(9)	$7^- \rightarrow 5^-$	–	–	6
1774.6	906.1	0.5(1)	$7^- \rightarrow 6^+$	–	–	3
1968.3	193.7	35.6(11)	$8^- \rightarrow 7^-$	0.7(1)	–	7

TABLE I. (*Continued.*)

E_i	E_γ	I_γ	$I_i^\pi \rightarrow I_f^\pi$	R_{AD}	A_P	Band no.
			Band 8			
2165.6	197.3	23.6(7)	$9^- \rightarrow 8^-$	–	–	7
2431.2	243.3	1.3(6)	$10^- \rightarrow 9^-$	–	–	7
2431.2	265.5	7.5(3)	$10^- \rightarrow 9^-$	0.6(1)	–	8
2431.2	462.8	4.3(3)	$10^- \rightarrow 8^-$	1.4(5)	–	7

$\Delta I = 1$ transitions are in agreement with both (i) almost pure unstretched $E2$ nature, and (ii) almost pure $M1$ multipolarity. Our linear polarization results, where available, did not have the needed precision to distinguish between these two options. It can be noted that the measured R_{AD} values of 0.8(3) for the $6^+ \rightarrow 6^+$ and $4^+ \rightarrow 4^+$ transitions linking the γ and the ground-state bands are too low for pure unstretched dipole nature and suggest considerable $E2$ admixture, in line with previous results where dominating $E2$ components were assigned [30].

The 4_3^+ band, Band 5, has also been extended with three new levels and eight new intraband and interband transitions. This band decays strongly to the 2_2^+ γ band. There are also three weak direct decays toward the ground-state band. In contrast to the 2_2^+ γ band, the intraband $\Delta I = 1$ transitions are relatively strong with relative intensity of $\approx 30\%$ of the corresponding intraband $E2$ transitions. Gated spectra illustrating the transitions of Band 5 are shown in Fig. 4. The spectra were obtained by placing gates on the two previously reported γ rays of 208 and 585 keV, and on the newly observed 518-keV γ ray. The R_{AD} values for the intraband 432-, 455-, and 518-keV transitions suggest quadrupole nature. The measured R_{AD} value of 1.3(2) for the previously reported 208-keV transition

is too large for a pure $\Delta I = 1$ transition, but suggests a mixed $M1 + E2$ nature with a dominant $E2$ component for this transition, in agreement with the available evaluated experimental data [30].

The previously reported transitions of the ground-state band (Band 3) and the high-K negative-parity bands (Bands 6–8) were also observed in our data. The levels near the bandheads of the negative-parity bands are shown in Fig. 1. Two new transitions with energies of 212 and 1195 keV were added.

The transitions shown in Fig. 1 as Bands 2a, 2b, and 2c were previously interpreted as one band associated with $\nu i_{13/2}^2$ configuration, with $K = 10$, and tilted nature [28]. The transitions were confirmed in the present work. However, based on an examination of the decay pattern of this band we propose that near $I^\pi = 14^+$ the band changes its nature. Indeed, while the lower-spin states are connected with strong intraband dipole transitions (which is a feature of a high-K band), dipole transitions could not be observed for the higher spin states. In addition the odd- and even-spin sequences at higher spins show energy staggering with large magnitude, which is not expected for a high-K band. Furthermore, while the 10^+ bandhead level of Band 2 decays strongly toward the $K = 9$ band and very weakly towards the ground-state band (in agreement with the high-K nature of the 10^+ bandhead), the decay pattern at higher spins changes, and
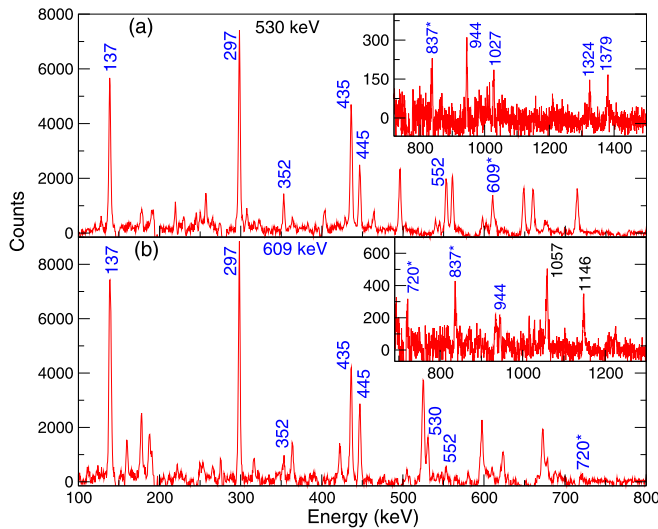
FIG. 2. Gated spectra showing the transitions of Band 1, obtained by placing gates on the (a) 530- and (b) 609-keV transitions. The transitions in blue are coincidence members of Bands 1 and 3. The ones in black belong to the 2_2^+ γ band. The new transitions are marked with an asterisk. The insets show the high-energy parts of these gated spectra.
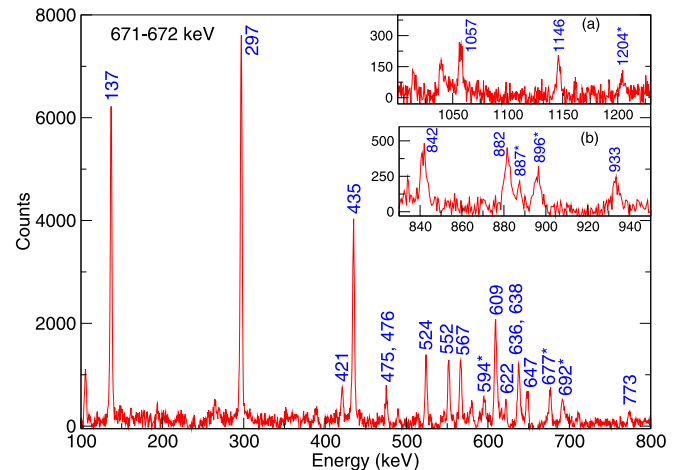
FIG. 3. A coincidence spectrum showing the transitions of Band 4, obtained by placing a gate on the 671-672-keV doublet transition. The transitions in blue are coincidence members of Bands 3 and 4. The new transitions are marked with an asterisk. The insets show the high-energy parts of this gated spectrum.
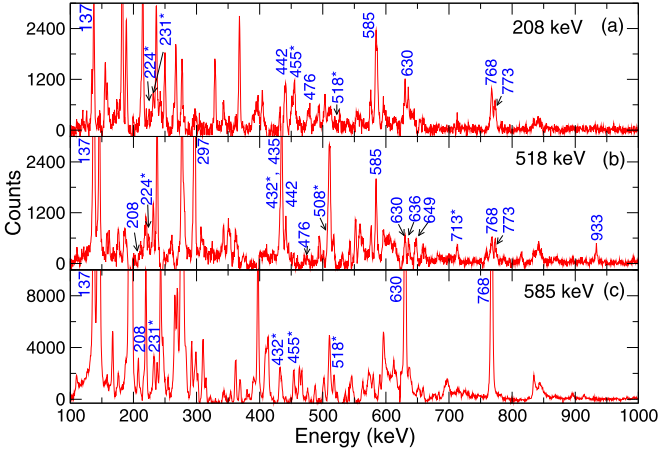
FIG. 4. Spectra, gated on (a) 208-keV, (b) 518-keV, (c) and 585-keV γ-ray transitions, showing the coincidence γ-ray energies of the ground-state, 2_2^+ and 4_3^+ bands. The new transitions of the 4_3^+ band are marked with an asterisk.

the 14^+ state decays predominantly towards the ground-state band. The strength of the decaying transitions measured in this work yield a value of $B(E2; 659)/B(E2; 401) = 1.9(3)$. This shows that the decay probability from the 14^+ state toward the ground-state band is about twice as large as that for the decay toward Band 2a. Therefore the intrinsic nature of the 14^+ state is closer to that of the ground-state band. The features of the higher-spin states with $I \geqslant 14$ resemble a low-K structure, such as a decoupled band, with its favored and unfavored signatures. Such an interpretation would be consistent with the lower excitation energy of the even-spin sequence with respect to the odd-spin sequence, and with the observation of weak (or missing) dipole transitions between the two sequences. Based on these considerations and the decay out patterns, the high-spin states were assigned as Bands 2b and 2c; see Fig. 1. Most probably these bands are associated with $\nu i_{13/2}$ nature, where the angular momenta of the two odd neutrons are aligned along the rotational axis, while the low-spin part of the band, Band 2a, corresponds to high-K $\nu i_{13/2}$ configuration, as previously proposed [28].

IV. DISCUSSION

The experimental excitation energies of the observed positive-parity bands built on the 0_1^+, 0_2^+, 2_2^+, and 4_3^+ states in ^{186}Os were compared with those of the neighboring e-e $^{182-192}$Os isotopes, and the systematic trends are presented in Appendix 1. In addition the links between the different bands are discussed in relation to simple models based on a harmonic vibration and a rigid rotation. Furthermore, the experimental results were compared to calculations using the model of a five-dimensional collective Hamiltonian based on the covariant density functional theory (5DCH-CDFT. Such calculations were applied in the 160 mass region, [6,8,9,14–19,31–36] and for the nuclei in the Er–Pt region [26].

A. Linking transitions between the bands of ^{186}Os

The e-e Os isotopes are considered as one of the best regions where the γ degree of freedom plays an important role in generating positive-parity bands at low excitation energy. A simple description based on a coupling of rotational and vibrational motion considers a deformed axially symmetric nucleus that can simultaneously rotate and vibrate. The vibrations are described by small harmonic oscillations with respect to the quadrupole deformation β and the triaxiality parameter γ. Within the adiabatic approach the rotational and vibrational degrees of freedom can be regarded as independent, and the nuclear states have excitation energy of

$$E(n_\beta, n_\gamma, K, I) = A[I(I+1) - K^2]$$
$$+ (n_\beta + 1/2)E_\beta + (n_\gamma + 1/2)E_\gamma, \quad (3)$$

where n_β and n_γ are the numbers of excited β and γ vibrational phonons, A is the rotational parameter inversely proportional to the moment of inertia, K is the projection of the total angular momentum along the symmetry axis, and $E_\beta(E_\gamma)$ are excitation energies carried by one β (γ) phonon. Within this interpretation the 2_2^+ γ band is produced by a coupling of one γ phonon, $n_\gamma = 1$, with the rotation of the deformed nucleus. The 4_3^+ γ band corresponds to a coupling of two γ phonons, $n_\gamma = 2$, with the rotation of the deformed nucleus. The energy of the 4_3^+ γ bandhead is expected to be twice as large as the energy of the 2_2^+ bandhead and corresponds to two γ phonons. Each γ phonon carries angular momentum of $2\hbar$, thus the 2_2^+ and the the 4_3^+ γ bands correspond to $K = 2$ and $K = 4$, respectively. The projection of the total angular momentum K is conserved. For more details on this description, see Ref. [2].

This interpretation implies several specific features of the rotational bands, for instance,

(a) The γ bands consist of even- and odd-spin sequences, and all $\Delta I = 1$ and $\Delta I = 2$ intraband transitions in both the 2_2^+ and the 4_3^+ bands would have strong $B(E2)$ components of similar magnitude to the $B(E2)$ rates of the intraband transitions in the ground-state band.

(b) As K is conserved, the decays between different bands would follow the K-selection rule, that is they would be with multipole order $L \geqslant \Delta K$. That implies that the $\Delta K = 2$ decays between the 2_2^+ γ band and the ground-state band and between the 4_3^+ and the 2_2^+ γ bands can proceed through transitions with multipole order $L \geqslant 2$. Therefore the $I \to I$ and the $I \to I - 1$ linking transitions would be of pure unstretched $E2$ nature (without $M1$ component). In addition the $\Delta K = 4$ decays from the 4_3^+ to the ground-state bands would be forbidden. Moreover the decays between the two-quasiparticle negative-parity bands and the two γ bands should obey the same rule, $L \geqslant \Delta K$.

We have examined the features of the level scheme of ^{186}Os shown in Fig. 1 with respect to these expectations. The intraband transitions in the 2_2^+ γ band are in general weak. In particular we did not observe intraband $\Delta I = 1$ transitions and restricted the branching intensities of the previously reported 143-, 161- and 215-keV transitions to below

1%. Despite their very low intensity, if these transitions have dominant $E2$ nature, the corresponding $B(E2)$ strength could still be of the same order of magnitude as the $B(E2)$ reduced transition probabilities in the ground-state band.

The observed decays out of the rotational bands suggest that in general the K-selection rule is followed. For instance the previously measured mixing ratios of the $\Delta I = 1$ and $\Delta I = 0$ transitions linking the 2_2^+ γ band and the ground-state band (e.g., the 476-, 773-, 636-, 407-, 842-, and 622-keV transitions) correspond to almost pure unstretched $E2$ nature with an $E2$ component of more than 99% [30]. Our data revealed several new linking transitions at higher spins. Our angular distribution ratio and linear polarization data for the $I \rightarrow I - 1$ linking transitions support the assigned spins and parities, and are consistent with both almost pure stretched $M1$ and almost pure unstretched $E2$ multipolarities. Similarly the previously measured mixing ratios for the $\Delta I = 1$ and $\Delta I = 0$ transitions linking the 4_3^+ and the 2_2^+ bands of 282-, 442-, and 489 keV support almost pure (>99%) unstretched $E2$ multipolarity. We could not deduce the values of the mixing ratios for the new higher-spin linking transitions.

The almost pure $E2$ multipolarity for the linking transitions suggests that the K-selection rule is generally obeyed; however, some K-forbidden decays are also present. For instance such transitions are (i) the decays from the 4_3^+ bandhead towards the ground-state band corresponding to $\Delta K = 4$; (ii) the $\Delta K = 10$ decay from the 10_2^+ bandhead of Band 2a toward the ground-state band; (iii) the $\Delta K = 3$ and $\Delta K = 5$ decays from the 5_1^- and 6_1^- states of Band 6 toward the 2_2^+ γ and the ground-state bands; and (iv) the $\Delta K = 7$ decay from the 7_1^- bandhead of Band 7 to the ground-state band. These K-forbidden decays are marked with blue asterisks in Fig. 1.

These K-forbidden transitions are observed, however, their intensities are considerably reduced. For instance,

(i) The forbidden $\Delta K = 4$ decays from the 4_3^+ band head are very weak. The $B(E2)$ reduced transition probability measured in this work for the 1215-keV $\Delta K = 4$ transition is 8.79×10^{-4} times the $B(E2)$ probability for the allowed 584-keV $\Delta K = 2$ transition.

(ii) Among the $5_1^- \rightarrow 4^+$ decays out of the $K = 5$ two-quasiparticle band, the reduced $B(E1)$ transition probability is largest for the decay to the 4_3^+ level with $K = 4$, which corresponds to $\Delta K = 1$ decay. The two other $5_1^- \rightarrow 4^+$ decays are forbidden by the K-selection rule and their observed intensity is strongly reduced, with $B(E1, 558)/B(E1, 277) = 3.6 \times 10^{-2}$ for the $\Delta K = 3$ decay to the 2_2^+ γ band and with $B(E1, 1195)/B(E1, 277) = 4.6 \times 10^{-5}$ for the $\Delta K = 5$ decay to the ground-state band.

(iii) The decays from the high-K bands, e.g., $K \geqslant 5$, toward the ground-state band are also generally weak. For instance, the γ-ray intensities of the 903-, 906-, and 1142-keV transitions are approximately 18%, 2%, and 3%, respectively, of the intensities of the strongest transitions depopulating their corresponding initial levels.

To summarize, the observed features of the rotational bands provide evidence supporting a description in terms of conservation of K, although it seems that allowing for some (small) K admixtures will also be appropriate.

Further information on the magnitude of the K-mixing can be obtained by analyzing the Alaga ratios and studying the features of the corresponding Mikhailov plots [37]. The Alaga ratios represent the ratios of the $B(E2)$ strengths of two transitions decaying from the same level towards states of another band, for instance, $B(E2 : I_\gamma^+ \rightarrow (I - 2)_g)/B(E2 : I_\gamma^+ \rightarrow I_g^+)$. The experimental values for these ratios for the 2_2^+, 4_2^+, and 6_2^+ states of the γ band are 0.43(4), 0.12(1), 0.06(1), respectively, which are lower than the theoretical values of 0.70, 0.34, 0.27 expected by the vibrational model. The difference indicates some K mixing in the states of the 2^+ γ band. The Mikhailov plot based on the available experimental data for these states shows a slope and thus indicates K mixing, (see also Ref. [38]). However, it remains unclear how substantial is the K mixing for these states and whether it can be regarded as a small perturbation.

Nuclear states with the same spins and parities and with similar excitation energies can mix. If such states correspond to different K values, where K is conserved, the mixing would generate admixtures in the corresponding K values. This mechanism can cause mixing in states from bands with the same parities, but it seems unclear whether it can explain all observed forbidden decays, particularly those involving states with different parities.

An alternative mechanism that generates K-admixtures can occur if the nuclear shape has nonaxial deformation. Triaxial nuclei rotate and produce excited bands, for which K is only approximately conserved near the bandhead and up to moderate spins. Calculations in terms of triaxial-rotor model (TRM) and triaxial projected shell model (TPSM) have been carried out previously for the Os isotopes [23,39]. The suitability of this model for the 2_2^+ γ band is strongly supported by the experimental data on the excitation energies, which shows a good agreement with the parameter-free prediction of the model that $E_{\text{exc}}(2_1^+) + E_{\text{exc}}(2_2^+) = E_{\text{exc}}(3_1^+)$. In the following subsection we present our TRM calculations for ^{186}Os and illustrate the partial conservation of the K values within this model.

B. Triaxial-rotor model for ^{186}Os

Calculations for ^{186}Os were carried out with a triaxial-rotor model (TRM) [4,5] where the nucleus was assumed to have a triaxial shape with quadrupole deformation $\beta = 0.21$, triaxiality $\gamma = 20°$. The moments of inertia followed an irrotational-flow trend as a function of the γ deformation, while their spin dependence was described using Harris parameters of $J_0 = 18.5$ MeV^{-1} and $J_1 = 200$ MeV^{-3}.

Figures 5(a) and 5(c) compare the experimental excitation energies for the ground-state and the 2_2^+ and 4_3^+ excited bands with the TRM calculations. There are two important disagreements with the experimental data, e.g., (i) the calculated relative excitation energies between the bands increase as a function of the spin, and (ii) the calculated 2_2^+ γ band shows significant energy staggering towards higher spins. Both of
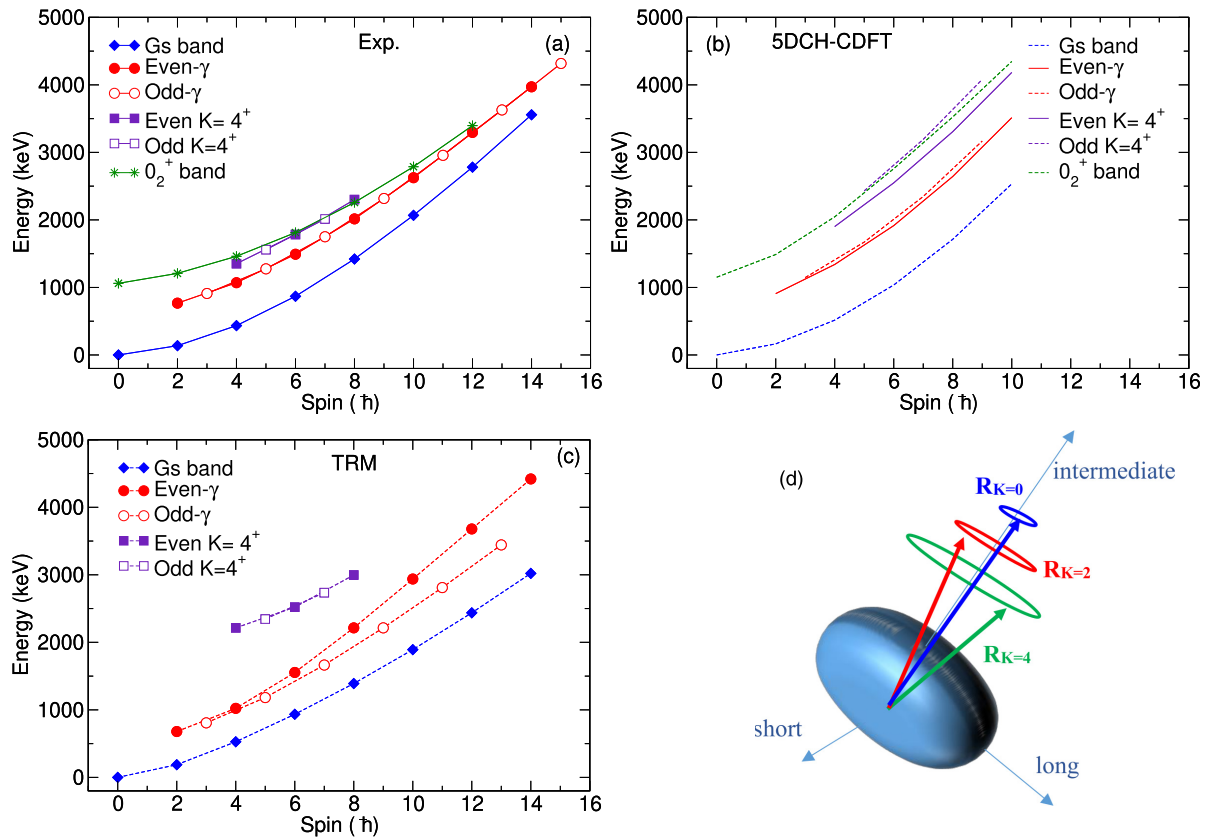
FIG. 5. Excitation energies for the ground-state, 2_2^+, and 4_3^+ γ bands in ^{186}Os, obtained from (a) experimental data, (b) 5DCH-CDFT model, and (c) TRM calculations. The rotation of a triaxial nucleus resembles the precession of a rotating top, with the rotational angular momentum R precessing around the intermediate nuclear axis, as illustrated in panel (d). The rotational angular momentum around the long and short nuclear axes generates a tilt of the total rotational angular momentum.

these predictions reflect general features of the triaxial-rotor model. The former follows the model assumption that all rotational bands have the same moments of inertia, but the observed decrease in the experimental relative excitation energies [see Fig. 5(a)] suggests that this assumption is not a good match to the data for ^{186}Os. It is also worth noting that the calculations do not give a good description of the energies of the 4_3^+ band; see Fig. 5(c). A model that adopts slightly larger moments of inertia for the excited bands would be more suitable. The energy staggering in the 2_2^+ γ band is discussed in detail in the next section.

Most interesting for us is that the model describes nuclear states that correspond to approximate conservation of K, where some mixture of K values is allowed. In general the triaxial-rotor model interprets the rotational bands as a precession of the intermediate nuclear axis, in a similar way as a rotating top precesses around the vertical direction. The ground-state band corresponds to precession with smallest tilt with respect to the intermediate axis, because the projection of the rotational angular momentum is almost entirely along the intermediate axis, and the projection along the long axis is $K = 0$; see Fig. 5(d). The 2_2^+ and 4_3^+ γ bands correspond to a gradual increase of the tilt of the precessing rotational angular momentum, $R_{K=2}$ and $R_{K=4}$, respectively, that corresponds to $K = 2$ and $K = 4$. This schematic description of the three-dimensional rotation of a triaxial nu-

cleus is valid near the bandheads of these bands, where K is approximately conserved, while at higher spins the mixing becomes important. To illustrate this mixing we have examined the wave functions of the states of the three bands; see Fig. 6.

The calculated wave functions of the states from the ground-state band are illustrated in Fig. 6(a). For each state with spin I the contributions of components with different values of K (where the rotational angular momentum is projected along the long axis) are represented by columns with different colors. For instance the wave function of the 2_1^+ state indicates that it is almost exclusively (more than 80%) associated with a component with $K = 0$ (see the blue column). Therefore the rotation is almost fully aligned along the intermediate axis. This component is dominant for the states of the ground-state band at low spins, supporting the approximate description of the ground-state states at low spins as $K = 0$ states. Similarly, the wave functions of the low-spin states of the 2_2^+ γ band correspond to dominant $K = 2$ contributions (the brown columns) in Fig. 6(b) and thus to precession around the intermediate axis with larger tilt than that for the ground-state band [see the sketch in Fig. 5(d)]. The calculated low-spin states from the 4_3^+ band are associated with dominant $K = 4$ contributions (the grey columns) in Fig. 6(c) and thus correspond to precession around the intermediate axis at a larger angle; see Fig. 5(d).
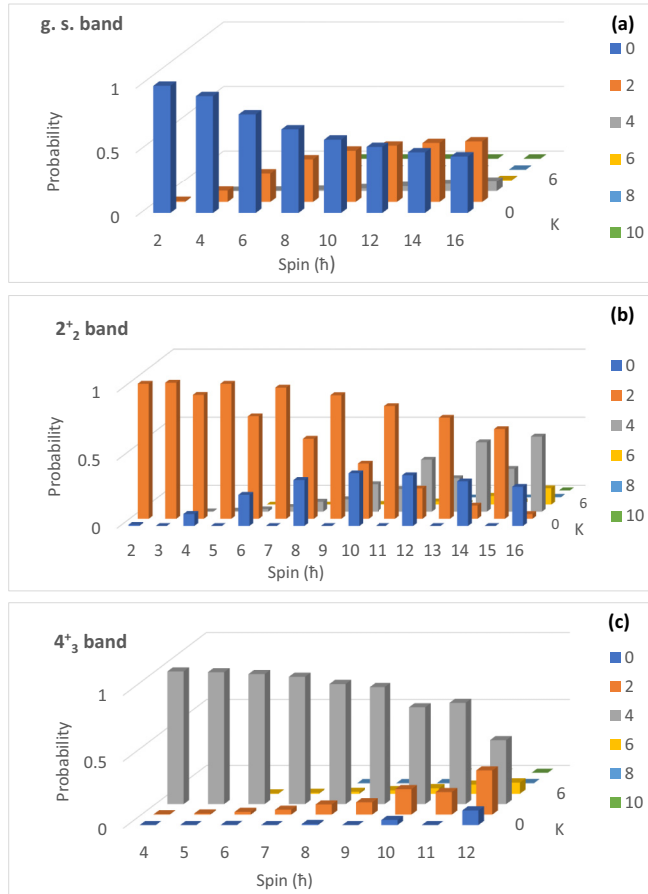
FIG. 6. The probability distributions of the wave functions for the states with spin I of the (a) ground-state, (b) 2_2^+, and (c) 4_3^+ bands. The wave functions are projected on the long axis. The values of K are shown on the *y* axis, and are also illustrated with different colous as listed in the legends.

In contrast to these well-defined dominant types of precession with $K = 0$, 2, and 4 for the ground-state, 2_2^+, and 4_3^+ bands, respectively, the high-spin states in these bands have large contributions from components with various K values.

This behavior highlights an important difference between the interpretations of these bands in terms of (i) small vibrations around axially symmetric shape, which preserves K, and assigns $K = 0$, $K = 2$, and $K = 4$ to the ground-state, 2_2^+, and 4_3^+ γ bands, respectively, and (ii) triaxial rotor, where K is approximately good near the bandheads and becomes strongly mixed at higher spins. Therefore within the former description the transitions linking bands with $\Delta K = 2$, (such as the 2_2^+ γ band and the ground-state band, or the 4_3^+ and 2_2^+ bands) should correspond to $L \geqslant \Delta K$ (therefore pure $E2$ character) both near the bandheads and at high spins as K is conserved. In contrast to that, the latter description allows for this requirement to be somewhat weaker near the bandheads, due to the approximate nature of the K conservation at low spins, while at high spins, where the states correspond to a mixture of various K values, the K-selection rule might not be obeyed. Therefore it is interesting to study the experimental data and test whether the linking transitions between the positive-parity

bands correspond to pure $E2$ nature including up to high spins, in line with a description within γ vibrations around an axially symmetric shape, or whether the linking transitions at high spins show a mixed $M1 + E2$ multipolarity, which would indicate that K is not well conserved and the nuclear shape might acquire some rigid triaxiality. Our measurements could not provide precise measurements of the mixing ratios of the linking transitions, but such study can be carried out in the future. In the following section results from the 5DCH-CDFT calculations are discussed.

C. Comparison with the 5DCH-CDFT calculations

Calculations assuming a rigid triaxial shape carried out within a triaxial-rotor model [23] and with the triaxial projected shell model [39] have reported quite good agreement with the available experimental data. On the other hand, a model that has the potential to consider both γ vibrations and rigid triaxial rotations could be better adapted for the Os isotopes. Systematic calculations within the 5DCH-CDFT model have been published recently for the nuclei in the Er–Pt region. The 5DCH-CDFT model [24,25] is a modern form of the Bohr Hamiltonian, which has been extended to allow large magnitude vibrations both in terms of β and γ in combination with a rotation of a nucleus with a deformed shape. Therefore the model can simultaneously treat the vibrational and rotational excitations of a triaxial or axially symmetric nucleus. The low-lying excitations of deformed nuclei can be described using a collective Hamiltonian with deformation-dependent parameters β and γ and three Euler angles $\Omega \equiv (\phi, \theta, \psi)$ defining the orientation of the intrinsic principal axes in the laboratory frame. The collective Hamiltonian is defined as

$$\hat{H}_{\text{coll}}(\beta, \gamma) = \hat{T}_{\text{vib}}(\beta, \gamma) + \hat{T}_{\text{rot}}(\beta, \gamma, \Omega) + V_{\text{coll}}(\beta, \gamma), \quad (4)$$

where $\hat{T}_{\text{vib}}(\beta, \gamma)$ is the vibrational kinetic energy, $\hat{T}_{\text{rot}}(\beta, \gamma, \Omega)$ is the rotational kinetic energy, and $V_{\text{coll}}(\beta, \gamma)$ is the collective potential. The diagonalization of this collective Hamiltonian produces the properties of the low-lying states in deformed nuclei. More details of the three terms of the equation can be found in Ref. [25]. The collective parameters are self-consistently determined by the microscopic CDFT calculations. In these calculations, the relativistic point-coupling energy functional PC-PK1 and the separable pairing force are respectively adopted in the particle-hole particle-particle channels. Solving the Dirac equation is achieved by expanding the Dirac spinor in terms of the three-dimensional harmonic oscillator basis with 16 major shells.

The triaxial mean-field states with deformation parameters $\beta \in [0.0, 0.8]$ and $\gamma \in [0°, 60°]$ and steps of $\beta = 0.05$, and $\gamma = 6°$ are generated by imposing the parity $D2$ symmetry and time-reversal invariance in the quadrupole deformation constrained relativistic mean-field plus BCS calculation [25].

Potential energy surface (PES) calculations for ^{186}Os were used to calculate the wave functions of the states of the positive-parity rotational bands. These wave functions are discussed in more details in Appendix 2. Calculations within the 5DCH-CDFT model were also carried out for the 4_3^+ band in ^{186}Os. The density distributions calculated within
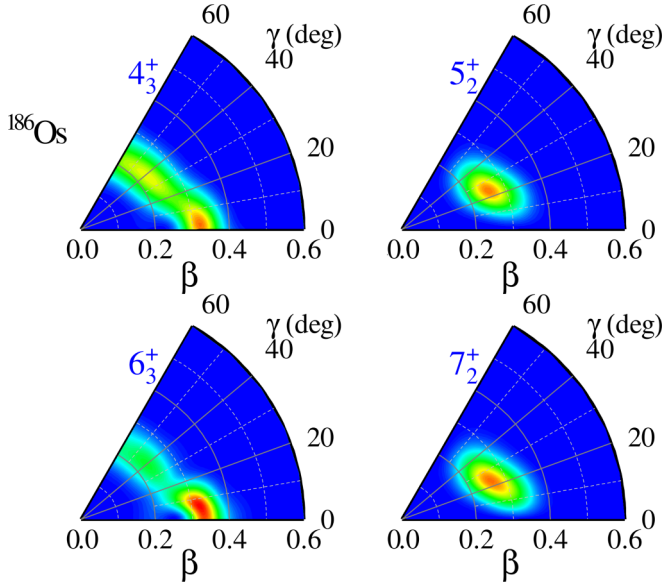
FIG. 7. Probability density distributions in the (β, γ) plane for the 4_3^+, 5_2^+, 6_3^+, and 7_2^+ states of the 4_3^+ band in ^{186}Os.

FIG. 8. Experimental staggering parameter $S(I)$ for the (a) 2_2^+ and (b) 4_3^+ bands in ^{186}Os, in comparison with the γ-vibrational, 5DCH-CDFT, γ-unstable, and TRM calculations.

this model for four states of this band are shown in Fig. 7. The results suggest that the even- and odd-spin members of this band have different nature. The wave functions of the odd-spin members predict a well-defined triaxial maximum at $\gamma \approx 25°$. The distributions indicate moderate softness with respect to β and γ (smaller than the softness of the ground state). In contrast to that, the probability distributions of the even-spin members correspond to a maximum at near axially symmetric prolate shape; however, the wave functions suggest considerable softness with respect to the γ degree of freedom. The predicted nature of the 4_3^+ state is, in particular, very similar to the γ-unstable Wilets-Jean model, where the potential seems almost independent of γ and oscillations between prolate and oblate deformation occur. The even-spin states, therefore, can be associated with large-magnitude γ vibrations coupled to rotation, while the odd-spin states, associated with well-defined triaxial shape, seem more likely to exhibit a three-dimensional rigid rotation.

A comparison of the calculated and experimental excitation energies for the low-energy positive-parity bands in ^{186}Os is shown in Figs. 5(a) and 5(b). There is a good agreement between the calculations and the experimental data in particular at low spins, except for the 4_3^+ band. At high spins it seems the calculated energies slightly overestimate the experimental data.

D. Energy staggering for the 2_2^+ and 4_3^+ bands

The energy staggering of the γ bands is often examined and compared with theoretical models to understand better the nature of these bands. The staggering parameter [40,41], $S(I)$, is defined as

$$S(I) = \frac{[E(I) - E(I-1)] - [E(I-1) - E(I-2)]}{E(2_1^+)}, \quad (5)$$

where $E(I)$, $E(I-1)$, and $E(I-2)$ represent the level energies of the γ bands at spins I, $I-1$, and $I-2$, respectively, and $E(2_1^+)$ is the energy of the first excited 2^+ state.

The staggering $S(I)$ has different behavior and different magnitude depending on the nature of the γ band. For instance a γ band described as large-magnitude γ vibrations within the γ-unstable model of Wilets-Jean exhibits large staggering that increases with spin for both the 2_2^+ and 4_3^+ bands; see Fig. 8. The magnitudes of the staggering calculated within this model well exceed the experimental observations. The triaxial-rotor model also produces a 2^+ γ band with large and increasing staggering, in disagreement with the magnitude and phase of the experimental data. On the other hand the staggering predicted by the TRM model for the 4^+ band is in very good agreement with the experimental data. The 5DCH-CDFT model reproduces both the phase and the magnitude of the staggering in the 2_2^+ band (although the latter is a bit overestimated), but the staggering predicted by this model for the 4_3^+ band is too large. The magnitude of the experimentally observed staggering in both bands is, in fact, best reproduced by a simple vibrational-rotational model, where the 2_2^+ and 4_3^+ bands are caused by one and two γ phonons coupled to the rotation of an axially symmetric nucleus. This description looks in general quite promising, because, in addition to successfully describing the staggering $S(I)$, it necessitates a stringent K-selection rule, which (based on the available data), is generally obeyed. Such simple model is not able to describe all features of the 2_2^+ and 4_3^+ bands. In fact the observation of a number of K-forbidden transitions implies that a mechanism that generates K admixtures (for instance triaxiality of the nuclear shape) is very probable. Furthermore, the 5DCH-CDFT model predicted well-defined triaxiality for the 2_2^+ band and for the odd-spin members of the 4_3^+ band, and γ softness for the even-spin members of this band. In addition, the 4_3^+ band is probably not entirely due to a collective excitation but involves significant single-particle contributions, as suggested by experiments on transfer reactions [21,22]. Further experimental and theoretical studies in the Os nuclei
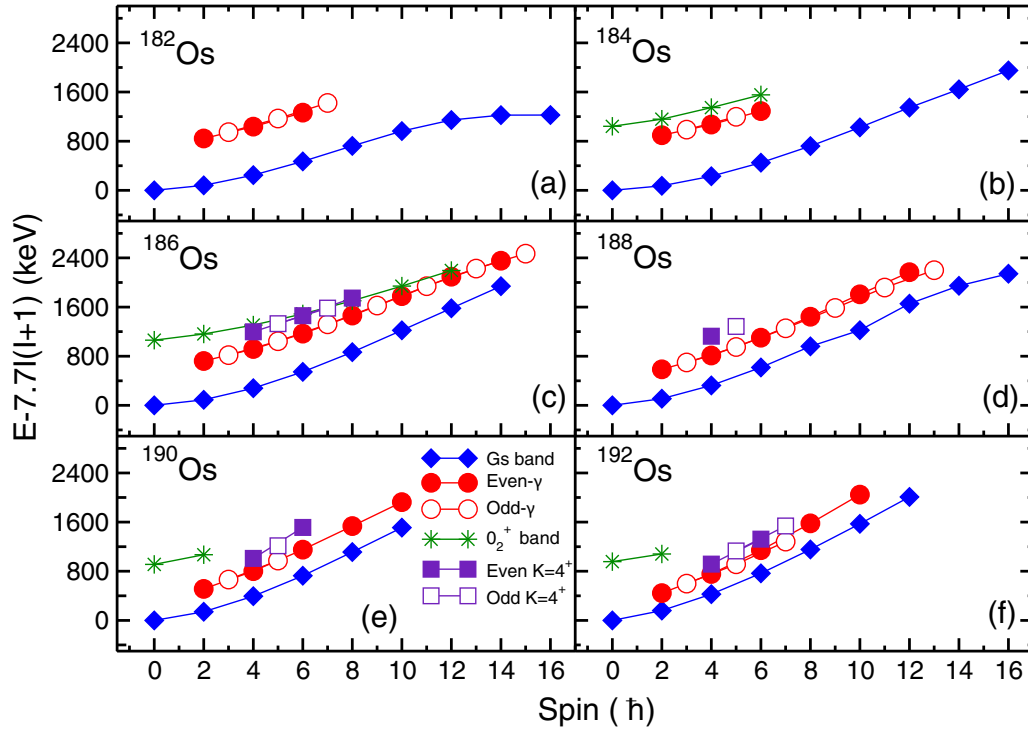
FIG. 9. Experimental level energies minus the energy of a rigid rotor, plotted as a function of spin for the ground-state, 0_2^+, 2_2^+, and 4_3^+ bands in the even-even $^{182-192}$Os isotopes.

are needed to reveal more details on the nature of the low-spin positive-parity bands. It seems to us that examining further the K-selection rule through precise measurements of the mixing ratios of transitions related to the 2_2^+ and 4_3^+ bands can shed more light on the nature of these bands.

V. CONCLUSION

Excited states in ^{186}Os have been studied following the ^{186}W(^{4}He, $4n$) ^{186}Os reaction. The experimental information on ^{186}Os has been improved by adding 20 new transitions to the decay scheme. Extensions to the bands built on the 0_2^+, 2_2^+, and 4_3^+ states were established and several new transitions linking these bands were observed. Spins and parities were assigned to the new levels based on angular distribution ratios and linear polarization measurements. The low-energy positive-parity bands in ^{186}Os were discussed in the context of a systematic comparison with the neighboring even-even $^{182-192}$Os isotopes and in terms of the small harmonic γ vibrations around axially symmetric shape, three-dimensional rotation of a triaxial nucleus, and within the 5DCH-CDFT model. The features of the observed bands support a compliance with the K-selection rule, although some K-forbidden decays were also observed, implying small K admixtures. The 5DCH-CDFT calculations provide a detailed description of the positive-parity bands in ^{186}Os, and are in very good agreement with the experimental data. The calculations assign a variety of different shapes to these bands, including an axially symmetric shape to the 0_1^+ and 0_2^+ bands and a triaxial shape to the 2_2^+ and 4_3^+ bands.

APPENDIX

1. Excitation energies and alignments of the low-energy positive-parity bands in $^{182-192}$Os

Comprehensive systematic studies [9,12–17,19,36] of the 2_2^+ γ bands showed that these bands in the $A \approx 160$ mass region track the ground-state band up to high spin, suggesting similar moments of inertia for these bands. These studies also showed that in some nuclei the 0_2^+ bands mix with the even-spin members of the 2_2^+ γ bands, resulting in a large signature splitting between the odd- and even-spin sequences of these γ bands.

The experimental level energies for the 0_1^+, 0_2^+, 2_2^+, and 4_3^+ bands in the e-e $^{182-192}$Os isotopes are shown in Fig. 9. As can be seen in this figure, the experimental information for the 0_2^+ bands is not known in the ^{182}Os and ^{188}Os nuclei, and little known in ^{184}Os, ^{190}Os, and ^{192}Os. This band is only well established in ^{184,186}Os. The present work extended this band in ^{186}Os. The slope of the excitation energy curve for this band in ^{186}Os is smaller compared to that of the other bands, indicating that its moment of inertia is somewhat higher; see Fig. 9(c). The bandhead energies of the 0_2^+ bands in the e-e
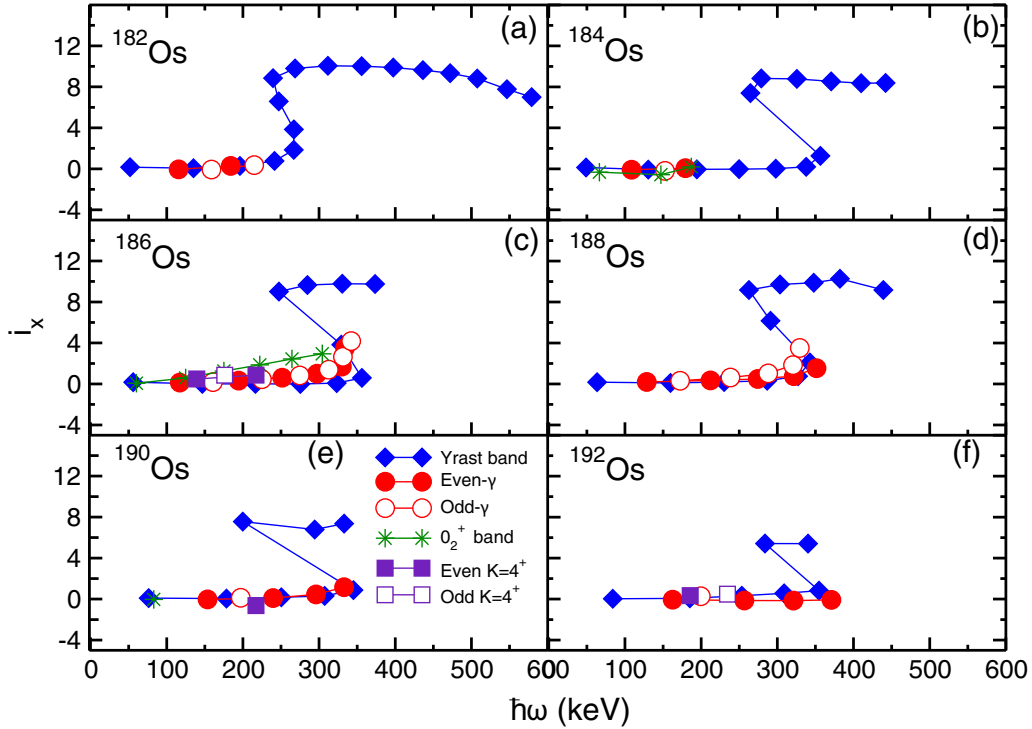
FIG. 10. Experimental alignments i_x, for the ground-state, 0_2^+, 2_2^+, and 4_3^+ bands in the even-even $^{182-192}$Os isotopes.

Os isotopes appear at an excitation energy of ≈ 900 keV, thus they lie higher than the bandheads of the 2_2^+ bands.

As shown in Fig. 9, the available experimental information on the 4_3^+ bands in the Os isotopes is scarce and the new data in ^{186}Os is the largest extension of this band to date. The observed slope of the excitation energy as a function of the spin is similar to that of the 2_2^+ γ band, implying a similar moment of inertia. There is the same similarity in the moment of inertia of these bands in ^{188,192}Os.

Figure 10 shows the experimental alignments i_x, plotted as a function of the rotational frequency ($\hbar\omega$). They are calculated assuming $K = 0$ for the 0_1^+ and 0_2^+ bands, $K = 2$ for the 2_2^+ γ bands, and $K = 4$ for the 4_3^+ bands. The alignment plots show that these bands have vanishing quasi-particle alignments. In the region of $\hbar\omega \approx 250$–350 keV ($I \approx 10$), backbends develop for the ground-state bands of all e-e $^{182-192}$Os isotopes. They were interpreted as due to the rotation alignments of a pair of $i_{13/2}$ neutrons.

2. Potential energy surfaces

Potential energy surface (PES) calculations for ^{186}Os are shown in the top panel of Fig. 11. The PES minimum corresponds to axially symmetric shape, although the calculations show softness with respect to the γ deformation.

These PESs were used to calculate the wave functions of the states of the positive-parity rotational bands. The 5DCH-CDFT model has an advantage with respect to the simple models discussed above, because it can calculate the nuclear shape for each state of the positive-parity rotational bands. The probability distributions for the ground-state band and for the bandheads of the 0_2^+ and 2_2^+ bands, projected in the

(β, γ) plane, are shown in the bottom panel of Fig. 11. The calculations indicate that both 0^+ states in ^{186}Os correspond to an axially symmetric shape, but the ground state exhibits a larger softness with respect to β and γ. The excited 0_2^+ state is associated with a very narrow distribution, which seems incompatible with β vibrations. The predicted quadrupole deformation for this 0_2^+ state is larger than the deformation for the ground state, implying that the excited 0_2^+ band is probably due to a shape coexistence. The predicted larger
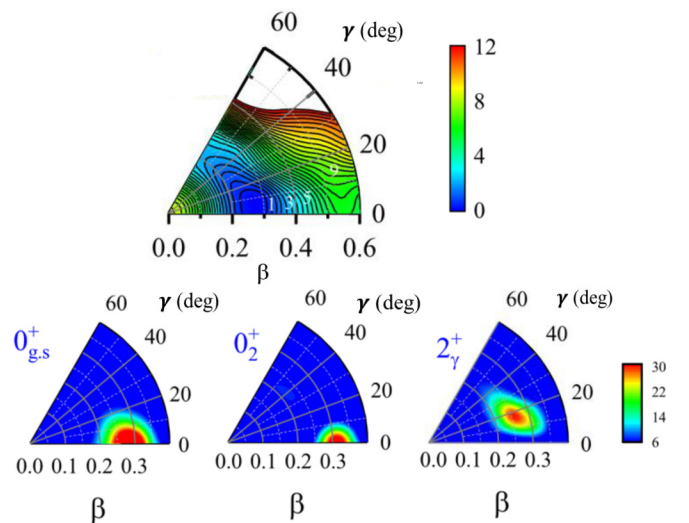
FIG. 11. Top: Potential-energy surface of ^{186}Os calculated in the (β, γ) plane. The energy difference between neighboring contours is 0.5 MeV. Bottom: Probability density distributions calculated in the (β, γ) plane for the 0_1^+, 0_2^+, and 2_2^+ states of ^{186}Os.

deformation is supported by the experimental data showing that the 0_2^+ band has a larger moment of inertia than the ground-state band; see panel (c) of Fig. 9. While the calcu- lations favor axially symmetric shape for the ground-state and the 0_2^+ bands, the shape predicted for the 2_2^+ band indicates a well-pronounced triaxiality with $\gamma \approx 15°$.

[1] A. Bohr and B. R. Mottelson, *Nuclear Structure, Volume II* (Word Scientific, Singapore, 1998), p. 363.

[2] D. J. Rowe and J. L. Wood, *Fundamentals of Nuclear Models: Foundational Models* (World Scientific, Singapore, 2010).

[3] A. S. Davydov and G. F. Philippov, Nucl. Phys. **8**, 237 (1958).

[4] P. B. Semmes and I. Ragnarsson, High spin physics and gamma-soft nuclei, in *Proceedings of the International Conference, Pittsburgh, 17–21 September 1990*, edited by J. X. Saladin, R. A. Sorensen, and C. M. Vincent (World Scientific, Singapore, 1990), p. 500.

[5] P. B. Semmes and I. Ragnarsson, in *Future Directions in Nuclear Physics with 4π Gamma Detection Systems of the New Generation, 4–16 March 1991, Strasbourg*, AIP Conf. Proc. No. 259 (AIP, New York, 1992), p. 566.

[6] P. E. Garrett, J. Phys. G: Nucl. Part. Phys. **27**, R1 (2001).

[7] J. F. Sharpey-Schafer, S. M. Mullins, R. A. Bark, J. Kau, F. Komati, E. A. Lawrie, J. J. Lawrie, T. E. Madiba, P. Maine, and A. Minkova, Eur. Phys. J. A **47**, 5 (2011).

[8] J. F. Sharpey-Schafer, T. E. Madiba, S. P. Bvumbi, E. A. Lawrie, J. J. Lawrie, A. Minkova, S. M. Mullins, P. Papka, D. G. Roux, and J. Timár, Eur. Phys. J. A **47**, 6 (2011).

[9] S. N. T. Majola, Z. Shi, B. Y. Song, Z. P. Li, S. Q. Zhang, R. A. Bark, J. F. Sharpey-Schafer, D. G. Aschman, S. P. Bvumbi, and T. D. Bucher, Phys. Rev. C **100**, 044324 (2019).

[10] J. F. Sharpey-Schafer, R. A. Bark, S. Bvumbi, E. A. Lawrie, J. J. Lawrie, T. E. Madiba, S. N. T. Majola, A. Minkova, S. M. Mullins, and P. Papka, Nucl. Phys. A **834**, 45c (2010).

[11] M. A. Sithole, E. A. Lawrie, L. Mdletshe, S. N. T. Majola, A. Kardan, T. D. Bucher, J. F. Sharpey-Schafer, J. J. Lawrie, S. S. Ntshangase, A. A. Avaa, R. A. Bark, M. V. Chisapi, P. Jones, S. Jongile, D. Kenfack, T. C. Khumalo, L. Makhathini, K. L. Malatji, B. Maqabuka, S. H. Mthembu, L. Msebi, A. A. Netshiya, G. ONeill, O. Shirinda, P. M. Someketa, and B. R. Zikhali, Phys. Rev. C **104**, 044326 (2021).

[12] S. N. T. Majola, M. A. Sithole, L. Mdletshe, D. Hartley, J. Timár, B. M. Nyakó, J. M. Allmond, R. A. Bark, and Beausang, Phys. Rev. C **101**, 044312 (2020).

[13] R. Bark, Z. Li, S. N. T. Majola, J. F. Sharpey-Schafer, Z. Shi, and S. Zhang, EPJ Web Conf. **178**, 02012 (2018).

[14] J. F. Sharpey-Schafer, R. A. Bark, S. P. Bvumbi, T. R. S. Dinoko, and S. N. T. Majola, Eur. Phys. J. A **55**, 15 (2019).

[15] S. Jehangir, G. H. Bhat, J. A. Sheikh, S. Frauendorf, S. N. T. Majola, P. A. Ganai, and J. F. Sharpey-Schafer, Phys. Rev. C **97**, 014310 (2018).

[16] L. Mdletshe, S. S. Ntshangase, J. F. Sharpey-Schafer, S. N. T. Majola, T. R. S. Dinoko, N. A. Khumalo, E. A. Lawrie, R. A. Bark, T. D. Bucher, and N. Erasmus, Eur. Phys. J. A **54**, 176 (2018).

[17] S. N. Majola, D. J. Hartley, L. L. Riedinger, J. F. Sharpey-Schafer, J. M. Allmond, C. Beausang, M. P. Carpenter, C. J. Chiara, N. Cooper, D. Curien, B. J. P. Gall, P. E. Garrett, R. V. F. Janssens, F. G. Kondev, W. D. Kulp, T. Lauritsen, E. A. McCutchan, D. Miller, J. Piot, N. Redon, M. A. Riley, J. Simpson, I. Stefanescu, V. Werner, X. Wang, J. L. Wood, C. H. Yu, and S. Zhu, Phys. Rev. C **91**, 034330 (2015).

[18] S. P. Bvumbi, J. F. Sharpey-Schafer, P. M. Jones, S. M. Mullins, B. M. Nyako, K. Juhasz, R. A. Bark, L. Bianco, D. M. Cullen, D. Curien, P. E. Garrett, P. T. Greenlees, J. Hirvonen, U. Jakobsson, J. Kau, F. Komati, R. Julin, S. Juutinen, S. Ketelhut, A. Korichi, E. A. Lawrie, J. J. Lawrie, M. Leino, T. E. Madiba, S. N. T. Majola, P. Maine, A. Minkova, N. J. Ncapayi, P. Nieminen, P. Peura, P. Rahkila, L. L. Riedinger, P. Ruotsalainen, J. Saren, C. Scholey, J. Sorri, S. Stolze, J. Timar, J. Uusitalo, and P. A. Vymers, Phys. Rev. C **87**, 044333 (2013).

[19] G. L. Zimba, S. P. Bvumbi, L. P. Masiteng, P. Jones, J. F. Sharpey-Schafer, S. N. T. Majola, T. S. Dinoko, O. Shirinda, J. J. Lawrie, and J. Easton, Eur. Phys. J. A **54**, 59 (2018).

[20] C. Y. Wu, D. Cline, T. Czosnyka, A. Backlin, C. Baktash, R. M. Diamond, G. D. Dracoulis, L. Hasselgren, H. Kluge, and B. Kotlinski, Nucl. Phys. A **607**, 178 (1996).

[21] D. G. Burke, Phys. Rev. Lett. **73**, 1899 (1994).

[22] D. G. Burke, Phys. Lett. B **406**, 200 (1997).

[23] J. M. Allmond, R. Zaballa, A. M. Oros-Peusquens, W. D. Kulp, and J. L. Wood, Phys. Rev. C **78**, 014302 (2008).

[24] Z. P. Li, T. Nikšić, D. Vretenar, J. Meng, G. A. Lalazissis, and P. Ring, Phys. Rev. C **79**, 054301 (2009).

[25] J. Xiang, Z. P. Li, Z. X. Li, J. M. Yaoa, and J. Meng, Nucl. Phys. A **873**, 1 (2012).

[26] X. Q. Yang, L. J. Wang, J. Xiang, X. Y. Wu, and Z. P. Li, Phys. Rev. C **103**, 054321 (2021).

[27] J. F. Sharpey-Schafer, Nucl. Phys. News **14**, 5 (2004).

[28] C. Wheldon, P. M. Walker, P. H. Regan, T. Saitoh, N. Hashimoto, G. Sletten, and E. R. Xu, Nucl. Phys. A **652**, 103 (1999).

[29] R. Spanhoff, H. Postma, and M. J. Canty, Phys. Rev. C **18**, 493 (1978).

[30] C. M. Baglin, Nucl. Data Sheets **99**, 1 (2003).

[31] D. Bucurescu, G. Graw, R. Hertenberger, H. F. Wirth, N. LoIudice, A. V. Sushkov, N. Y. Shirikova, Y. Sun, T. Faestermann, R. Krucken, M. Mahgoub, J. Jolie, P. vonBrentano, N. Braun, S. Heinze, O. Moller, D. Mucher, C. Scholl, R. F. Casten, and D. A. Meyer, Phys. Rev. C **73**, 064309 (2006).

[32] W. D. Kulp, J. L. Wood, P. E. Garrett, C. Y. Wu, D. Cline, J. M. Allmond, D. Bandyopadhyay, D. Dashdorj, S. N. Choudry, A. B. Hayes, H. Hua, M. G. Mynk, M. T. McEllistrem, C. J. McKay, J. N. Orce, R. Teng, and S. W. Yates, Phys. Rev. C **77**, 061301(R) (2008).

[33] N. Pietralla and O. M. Gorbachenko, Phys. Rev. C **70**, 011304(R) (2004).

[34] J. Smallcombe, P. J. Davies, C. J. Barton, D. G. Jenkins, L. L. Andersson, P. A. Butler, D. M. Cox, R.-D. Herzberg, A. Mistry, and E. Parr, Phys. Lett. B **732**, 161 (2014).

[35] W. D. Kulp, J. L. Wood, J. M. Allmond, J. Eimer, D. Furse, K. S. Krane, J. Loats, P. Schmelzenbach, C. J. Stapels, R. M. Larimer, E. B. Norman, and A. Piechaczek, Phys. Rev. C **76**, 034319 (2007).

[36] J. Ollier, J. Simpson, M. A. Riley, E. S. Paul, X. Wang, A. Aguilar, M. P. Carpenter, I. G. Darby, D. J. Hartley, R. V. F.

Janssens, F. G. Kondev, T. Lauritsen, P. J. Nolan, M. Petri, J. M. Rees, S. V. Rigby, C. Teal, J. Thomson, C. Unsworth, S. Zhu, A. Kardan, and I. Ragnarsson, Phys. Rev. C **83**, 044309 (2011).

[37] V. M. Mikhailov, Izv. Akad. Nauk SSSR, Ser. Fiz. **30**, 1334 (1966).

[38] C. Y. Wu and D. Cline, Phys. Lett. B **382**, 214 (1996).

[39] R. Gupta, A. Kumar, S. Singh, A. Bharti, G. H. Bhat, and J. A. Sheikh, Chin. J. Phys. **72**, 191 (2021).

[40] J. M. Rees, E. S. Paul, M. A. Riley, J. Simpson, A. D. Ayangeakaa, H. C. Boston, M. P. Carpenter, C. J. Chiara, U. Garg, D. J. Hartley, R. V. F. Janssens, D. S. Judson, F. G. Kondev, T. Lauritsen, N. M. Lumley, J. Matta, P. J. Nolan, J. Ollier, M. Petri, J. P. Revill, L. L. Riedinger, S. V. Rigby, C. Unsworth, X. Wang, and S. Zhu, Phys. Rev. C **83**, 044314 (2011).

[41] E. A. McCutchan, D. Bonatsos, N. V. Zamfir, and R. F. Casten, Phys. Rev. C **76**, 024306 (2007).